

Spectral function of the Holstein polaron at finite temperature

J. Bonča,^{1,2} S. A. Trugman,^{3,4} and M. Berciu^{5,6}

¹*J. Stefan Institute, 1000 Ljubljana, Slovenia*

²*Faculty of Mathematics and Physics, University of Ljubljana, 1000 Ljubljana, Slovenia*

³*Theoretical Division, Los Alamos National Laboratory, Los Alamos, New Mexico 87545, USA*

⁴*Center for Integrated Nanotechnologies, Los Alamos National Laboratory, Los Alamos, New Mexico 87545, USA*

⁵*Department of Physics and Astronomy, University of British Columbia, Vancouver, British Columbia, Canada, V6T 1Z1*

⁶*Stewart Blusson Quantum Matter Institute, University of British Columbia, Vancouver, British Columbia, Canada, V6T 1Z4*



(Received 27 February 2019; revised manuscript received 9 September 2019; published 18 September 2019)

We compute the Holstein polaron spectral function on a one-dimensional ring using the finite-temperature T Lanczos method. With increasing T additional features in the spectral function emerge even at temperatures below the phonon frequency. We observe a substantial spread of the spectral weight towards lower frequencies and the broadening of the quasiparticle (QP) peak. In the weak-coupling regime the QP peak merges with the continuum in the high- T limit. In the strong-coupling regime the main features of the low- T spectral function remain detectable up to the highest T used in our calculations. The effective polaron mass shows a nonmonotonic behavior as a function of T at small phonon frequency but increases with T at larger frequencies. The self-energy remains k independent even at elevated T in the frequency range corresponding to the polaron band, while at higher frequencies it develops a distinguishable k dependence. Analytical expressions for the first few frequency moments are derived, and they agree well with those extracted from numerical calculations in a wide- T regime.

DOI: [10.1103/PhysRevB.100.094307](https://doi.org/10.1103/PhysRevB.100.094307)

I. INTRODUCTION

The Holstein polaron model [1] represents one of the paradigmatic microscopic models in condensed-matter physics. Despite its simplicity it is often used to describe a variety of systems where a particle is coupled to localized bosonic degrees of freedom. Most often, it is applied to study the coupling between an electron and quantum lattice vibrations.

While ground-state properties of the Holstein polaron (HP) can be calculated with machine precision [2,3], computing spectral properties via the Green's function that contains the most complete information of a dressed quasiparticle is a considerably more challenging problem. Since early attempts to obtain the Green's function for electron-phonon coupled systems using diagrammatic techniques [4], many numerical approaches have been developed such as exact diagonalization approaches on finite lattices [5–9], cluster perturbation techniques [10], a variational approach based on an expansion in coherent states [11], diagrammatic Monte Carlo methods [12,13], and the momentum-averaged approximation [14–16].

While most approaches were limited to zero- T calculations, early finite- T results were obtained on a system with two sites using numerical calculations [17] as well as an analytical approach based on the continued fraction expansion [18]. Important progress has been achieved based on the dynamical mean-field approach that is exact in the infinite-dimensional limit [19] but lacks resolution in k space because the method is based on a mapping of the lattice problem onto a polaronic impurity model. The other significant investigation of the HP at finite- T is the study of the temperature-dependent mobility that was computed using numerical analytic contin-

uation combined with a diagrammatic and world line Monte Carlo method [20].

Despite significant advances in analytical as well as numerical techniques applied to tackle the HP model, the temperature dependence of the HP spectral functions remains so far unresolved. This is the problem solved in this paper. Among other open problems that we will address is the temperature dependence of the effective polaron mass for which early attempts based on Feynman's path-integral formalism gave conflicting results [21–23] and the k dependence of the self-energy at finite T . Our research was also motivated by recent measurements of the HP spectral function in a surface-doped layered semiconductor, MoS₂, where an unusual two-dimensional superconductivity has been reported [24].

II. MODEL AND METHOD

We analyze the Holstein model with a single electron in a one-dimensional chain of size L with periodic boundary conditions

$$H = -t_0 \sum_j (c_j^\dagger c_{j+1} + \text{H.c.}) - g \sum_j \hat{n}_j (a_j^\dagger + a_j) + \omega_0 \sum_j a_j^\dagger a_j, \quad (1)$$

where c_j^\dagger and a_j^\dagger are electron and phonon creation operators at site j , respectively, and $\hat{n}_j = c_j^\dagger c_j$ represents the electron density operator. ω_0 denotes a dispersionless optical phonon frequency, and t_0 is the nearest-neighbor hopping amplitude. We also introduce the dimensionless electron-phonon coupling strength $\lambda = g^2/2t_0\omega_0$.

To determine the spectral properties of the HP we have combined two methods. For the construction of the variational Hilbert space of the Hamiltonian in Eq. (1) we have used the approach originally introduced in Refs. [2,3] that led to numerically exact solutions of the polaron ground and low-lying excited-state properties. To compute temperature-dependent quantities we implemented the finite-temperature Lanczos method (FTLM) as described in Refs. [25,26]. The former method constructs the variational Hilbert space (VHS) starting from the single-electron Bloch state $c_{\mathbf{k}}^{\dagger}|\emptyset\rangle$ with no phonons on an infinite lattice. The VHS is then generated by applying the off-diagonal terms of Hamiltonian (1)

$$\{|\phi_{\mathbf{k},l}^{(N_h)}\rangle\} = (H_{\text{kin}} + H_g)^{N_h} c_{\mathbf{k}}^{\dagger}|\emptyset\rangle, \quad (2)$$

where H_{kin} and H_g correspond to the first and the second terms of the Hamiltonian in Eq. (1), respectively. Parameter N_h determines the size of the VHS. Typically, we take $N_h \gg L$.

The central quantity of this work is the single-electron spectral function defined via the corresponding retarded Green's function

$$A(\omega, k) = -\pi^{-1} \lim_{\eta \rightarrow 0^+} \mathcal{G}^R(\omega + i\eta, k), \quad (3)$$

where

$$\mathcal{G}^R(\omega, k) = \mathcal{Z}^{-1} \int_0^{\infty} dt e^{i\omega t} \sum_n e^{-\beta\epsilon_n^0} \langle \phi_n^0 | c_{\mathbf{k}}(t) c_{\mathbf{k}}^{\dagger}(0) | \phi_n^0 \rangle, \quad (4)$$

where ϕ_n^0 are multiphonon eigenstates of the Hamiltonian in Eq. (1) with no electron present in the system and ϵ_n^0 are corresponding energies. \mathcal{Z} is the partition function, and $c_{\mathbf{k}} = 1/\sqrt{L} \sum_{j=1}^L \exp(ikj) c_j$. Finally, we take advantage of the FTLM method [25], where the trace over all states in a given sector is replaced by the summation over random states $|r^0\rangle = \sum_{n=1}^{N_0} \alpha_n |\phi_n^0\rangle$, where α_n are distributed randomly and

$$A(\omega, k) = \mathcal{Z}^{-1} \sum_{r=1}^R \sum_{n=1}^{N_0} \sum_{j=1}^M e^{-\beta\epsilon_n^0} \langle r^0 | \phi_n^0 \rangle \langle \phi_n^0 | c_{\mathbf{k}} | \psi_j \rangle \times \langle \psi_j | c_{\mathbf{k}}^{\dagger} | r^0 \rangle \delta(\omega - \epsilon_j + \epsilon_n^0), \quad (5)$$

where $|\psi_j\rangle$ and ϵ_j are Lanczos wave functions and corresponding energies, respectively, in the subspace with one electron. Lanczos states are generated starting from states $c_{\mathbf{k}}^{\dagger}|r^0\rangle$. Furthermore, R represents the number of different random states, N_0 is the size of the Hilbert space in the zero-electron subspace, and M is the number of Lanczos iterations. We have used typically $M = 500$ Lanczos iterations combined with the Gram-Schmidt orthogonalization procedure to avoid spurious nonorthogonal states that appear due to round-off errors, introduced by the finite-precision arithmetics when using large values of M . The Lorentzian form of the δ functions with the half width at half maximum (HWHM) η was used for graphic representations of $A(k, \omega)$. In order to test our results we have derived exact expressions for the first few frequency moments that are free from finite-size effects. Frequency moments obtained from spectral functions agree well with their analytical counterparts in the whole temperature regime up to $T \sim 2\omega_0$ [16,27]. In Appendix B we further elaborate on the extent of finite-size effects by comparing spectral functions obtained from two distinctly different system sizes.

For the presentation of density plots shown later in this paper we have expanded calculations from using only periodic boundary conditions towards the so-called twisted boundary conditions [28–30], representing a magnetic flux penetrating the ring. This procedure allowed us to continuously connect discrete k points. In this approach the kinetic energy term in Eq. (1) is transformed to

$$H_{\text{kin}} = -t_0 \sum_j (c_j^{\dagger} c_{j+1} e^{i\theta} + \text{H.c.}). \quad (6)$$

For the system of free electrons such a transformation leads to the dispersion relation $\epsilon(k, \theta) = -2t_0 \cos(k + \theta)$, where θ represents a magnetic flux that penetrates the ring $\phi_m = \theta L/2\pi$ in units of h/e_0 . In the case of free electrons despite the calculation on a finite ring of size L an exact and continuous dispersion relation $\epsilon(k, \theta)$ can be obtained since discrete k points $k_n = 2\pi n/L$ can be smoothly connected by choosing $\theta \in [0, 2\pi/L]$. Reducing finite-size effects using twisted boundary conditions was also successfully applied to interacting systems with finite electron density [28–30].

III. RESULTS

A. Spectral functions

In Fig. 1(a) we present $A(\omega, k = 0)$ in the weak electron-phonon (EP) coupling regime, i.e., at $\lambda = 0.5$ for different values of temperature. At small $T = 0.1$ our results qualitatively agree with those obtained using cluster perturbation theory [10]. A well pronounced quasiparticle (QP) peak is located at $\omega_{\text{QP}} \sim -2.5$, followed by a smaller peak located around $\omega = \omega_{\text{QP}} + \omega_0$ that represents states composed of a polaron with an additional one-phonon excitation. It is worth noting that since the polaron peak is due to a single-polaron state, its HWHM is given by the artificial damping parameter η . In contrast, peaks at higher frequencies possess a finite width since they represent states in the continuum (for $L \rightarrow \infty$). With increasing $T \gtrsim 0.2$ two prominent features become visible. First, a pronounced structure appears below the QP peak, and second, the QP peak obtains a finite width, which on a small system emerges as a series of discrete peaks that materialize in the vicinity of the QP peak. At temperatures of the order of the phonon frequency, i.e., around $T \sim \omega_0$ the QP peak becomes indistinguishable from other parts of the spectra.

In the intermediate-coupling regime at $\lambda = 1$, presented in Fig. 1(b), we observe an interesting detail. At first glance it seems as if the QP, located at low T at $\omega_{\text{QP}} \sim -3.0$, shifts towards larger ω with increasing T . However, a closer inspection reveals that there is a shift of spectral weight from the QP peak towards a peak that at finite T emerges around $\omega \sim \omega_{\text{QP}} + 0.1$, as revealed in the inset of Fig. 1(b). In the thermodynamic limit such a process would appear as a gradual shift of the QP peak towards higher frequencies where a continuous set of peaks would emerge just above ω_{QP} that would support the shifted QP spectral weight.

In Fig. 1(c) we show $A(\omega, k = 0)$ in the strong-coupling regime, i.e., at $\lambda = 2$, where the QP peak appears at $\omega_{\text{QP}} \sim -4.4$. The most peculiar property in this case is the appearance of a well-pronounced peak above the QP one at a frequency that is below the threshold value for the onset of the continuum above the polaron band, e.g., at $\omega \sim$

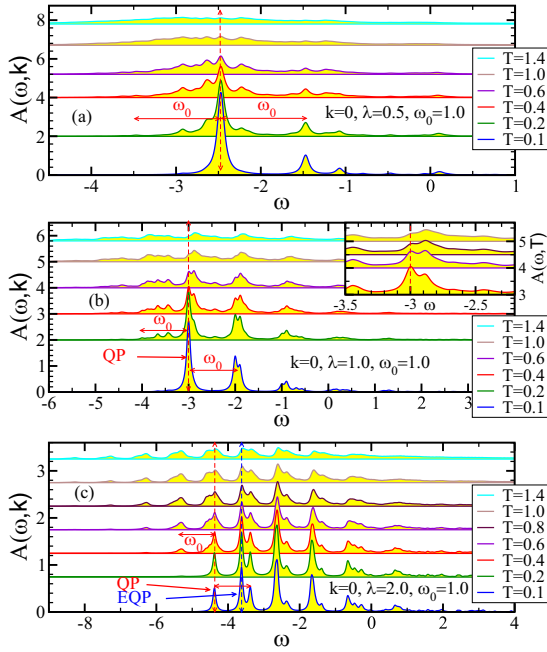


FIG. 1. $A(\omega, k = 0)$ at $\omega_0 = 1.0$ computed for $\lambda = 0.5$ through $\lambda = 2.0$ from (a) to (c). Temperature is measured in units of the hopping $t_0 = 1$. In this and all subsequent figures we have used the following parameters when generating the variational Hilbert space: $N_h = 22$, $L = 6$, $\eta = 0.05$, and $M = 500$. The Hilbert space spans over $N_1 \sim 120\,000$ states in the subspace of one electron and $N_0 = 23\,000$ different phonon degrees of freedom, taking into account all translationally invariant states in the zero-electron case. We have sampled over $R = 90$ distinct initial random states and all k sectors. Horizontal red lines with arrows on both sides indicate the corresponding ω_0 . Red vertical dashed lines point towards positions of QP peaks, while the blue dashed line indicates the position of the EQP peak in (c).

$-3.6 < \omega_{QP} + \omega_0$, as also indicated in Fig. 1(b). This peak marks the so-called bound polaron state that appears in the strong-coupling regime and consists of an excited polaron: a polaron with an extra phonon excitation that is bound to the polaron. [2,10,16,31,32]. It emerges below the continuum, and the width of this excited QP peak (EQP) is at low $T = 0.1$ also given by η . As the temperature increases, both peaks obtain a finite width. Additional well-defined peaks emerge at finite T at $\omega = \omega_{QP} - n\omega_0$. In contrast to the weak-coupling limit where the spectrum becomes featureless at high T , well-defined peaks persist in the strong-coupling limit up to highest T . The broadening of the peaks is at high T limited by the width of the corresponding polaronic bands. This structure of well-separated peaks that do not broaden with increasing T bears a similarity to the spectral function of a single-site problem, presented in Appendix C.

In summary, with increasing T there is a substantial shift of the spectral weight towards frequencies below the QP peak, i.e., $\omega < \omega_{QP}$. This effect becomes more pronounced with increasing λ . However, the center of the spectra, as defined through the first frequency moment, $M_1(k) = \int_{-\infty}^{\infty} \omega A(\omega, k) d\omega = -2t_0 \cos(k)$, remains independent of T , as further elaborated upon in Sec. III C. Spectral functions at

$k = \pi$ are displayed in various parameter regimes and elaborated in Appendix A. Next, we show in Fig. 2 density plots representing $A(\omega, k)$ in the entire Brillouin zone (BZ) in the intermediate-coupling regime $\lambda = 1$. We focus first on $\omega_0 = 1$ and small $T/\omega_0 = 0.1$, where the polaron band is clearly observed, although its QP weight strongly diminishes towards $k = \pi$, in agreement with many previous zero- T approaches [9,10,14–16]. The incoherent part of the spectra starts at $\omega_{QP} + \omega_0$. It is rather intriguing that the incoherent spectra around the center of the BZ almost replicate the polaron band. In the case of $\omega_0 = 0.5$, as shown in Fig 2(e), there exist two such well-defined replica bands inside the polaron plus one- and two-phonon continua. The incoherent part of the spectra at higher ω mimics rather closely the dispersion of the free-electron band, with a slightly expanded bandwidth.

To more quantitatively understand the nature of the continuum above the polaron band we show in Fig. 2(a) with dashed lines the zero- T polaron dispersion $\epsilon_{QP}(k)$ as well as $\epsilon_{QP}(k) + \omega_0$. In contrast to the polaron band that precisely follows $\epsilon_{QP}(k)$, the polaron plus one-phonon continuum follows the shifted dispersion relation only close to the center of the BZ, resembling a long-lived resonance inside the continuum. We also note that despite using a relatively small system size in order to allow for additional phonon excitations, in the low- T limit $A(\omega, k)$ agrees exceptionally well with the zero- T results from the cluster perturbation theory [10] as well as the momentum average approximation [16]. In addition, $\epsilon_{QP}(k)$, in this case obtained using twisted boundary conditions, quantitatively agrees with the dispersion relation obtained in Refs. [2,10], optimized for zero- T calculations, which furthermore justifies our approach.

The main focus of the present work is the evolution of $A(\omega, k)$ with T . Already at $T/\omega_0 = 0.3$ a noticeable spectral weight develops just below the polaron band. This part of the spectrum, located below the polaron ground-state energy, emerges from the process where an electron annihilates a thermally excited phonon. This enhanced spectral weight is predominantly located close to the center of the BZ, where the polaron has the largest quasiparticle weight. At even higher $T/\omega_0 \gtrsim 0.5$ a buildup of spectral weight is expected at even lower frequencies since an electron can annihilate more than one thermally excited phonon, as clearly seen from Figs. 2(c), 2(d), 2(g), and 2(h). While the overall effect of increasing T is to smear out the coherent as well as the incoherent parts of the spectra, the remnants of the QP band remain visible even at elevated $T/\omega_0 \sim 1$. Nevertheless, there are rather clear differences between $\omega_0 = 1$ and 0.5 spectra, as seen in Figs. 2(d) and 2(h). For $\omega_0 = 0.5$ the incoherent part of the spectrum merges with the polaron and quasibound polaron bands to form a structure, resembling the free-electron band but with a slightly larger bandwidth.

We have also followed the temperature evolution of subtle changes in the curvature of respective polaron bands to determine the T -dependent effective polaron mass m^* , as shown in Fig. 2(i) for different values of ω_0 . In the limit $T \rightarrow 0$ the results agree with zero- T approaches [2,9]. With increasing T we observe a clear increase of m^* for $\omega_0 = 1$ and 2 . In contrast, we find a very weak and nonmonotonic T dependence of m^* for small $\omega_0 = 0.5$ [33]. This result is in a qualitative agreement with the nonmonotonic temperature

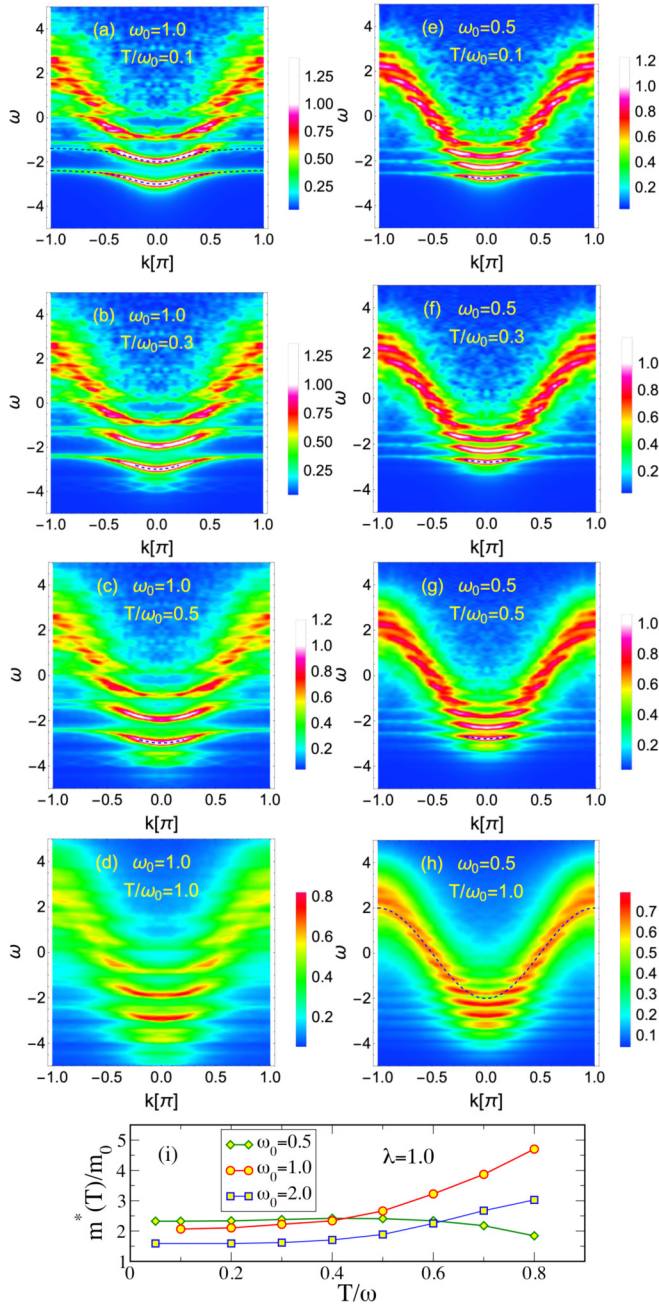


FIG. 2. $A(\omega, k)$ for $\lambda = 1$ vs different values of T/ω_0 and $\omega_0 = 1$ in (a)–(d) and $\omega_0 = 0.5$ in (e)–(h). The same size of the system was used as in Fig. 1. In addition we have used twisted boundary conditions to compute $A(\omega, k)$ at 25 equally spaced k points in the interval $k \in [0, \pi]$ with increments of $\Delta k = \pi/24$. Note that in all plots from (a) to (h) the same color coding was used to enable direct comparison between different cases. In (h) a free-electron band $\epsilon(k) = -2t_0 \cos(k)$ is shown using a dashed line as a guide to the eye. Lorentzian broadening $\eta = 0.05$ was used in all cases. In (i) we display m^*/m_0 , where $m_0 = 1/2t_0$ is the free-electron mass, obtained from fits to the polaron band using the analytical form $\epsilon_f(k) = \sum_n a_n \cos(nk)$, up to $n = 3$, shown as dashed lines in (a)–(c) and (e)–(g).

renormalization of the effective polaron band found on a two-site system [17].

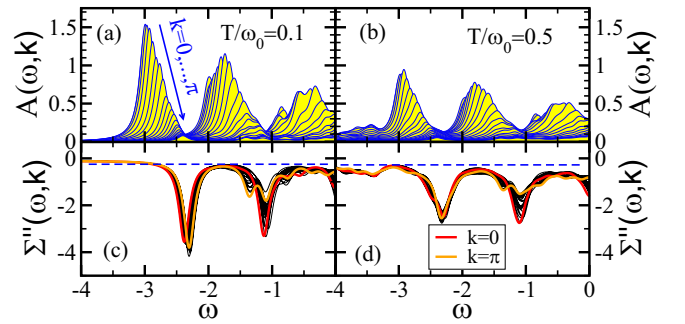


FIG. 3. $A(\omega, k)$ and $\Sigma(\omega, k)$ for $\lambda = \omega_0 = 1$ computed at values of $T/\omega_0 = 0.1$ in (a) and (c) and 0.5 in (b) and (d). The same size of the system was used as in Figs. 1 and 2. In each plot we present 25 curves computed at equally spaced k points in the interval $k \in [0, \pi]$ with increments of $\Delta k = \pi/24$. Lorentzian broadening $\eta = 0.05$ was used in all cases, which is also responsible for a small deviation from zero in (c) for $\omega \lesssim -2.7$.

B. Self-energies

In Fig. 3 we show a family of $A(\omega, k)$ for a set of $k \in [0, \pi]$ values together with the imaginary parts of corresponding self-energies $\Sigma''(\omega, k)$ extracted from the relation $\mathcal{G}^R(\omega, k) = 1/[\omega - \epsilon(k) - \Sigma(\omega, k)]$, where $\epsilon(k) = -2t_0 \cos(k)$. We focus mainly on the k dependence of $\Sigma''(\omega, k)$ and its evolution with T . At low $T = 0.1$ and low ω we observe nearly k independent $\Sigma''(\omega, k)$ [see Fig. 3(c)], which stands in sharp contrast to the k dependence of $A(\omega, k)$, shown in Fig. 3(a). Moreover, $\Sigma''(\omega, k) \sim 0$ through the whole polaron band, indicating the band is perfectly coherent. $\Sigma''(\omega, k)$ remains rather small also through the lower part of the polaron plus one-phonon continuum; however, it substantially increases towards $\omega \sim -1.4$, where it also develops a noticeable k dependence in accordance with the density plot shown in Fig. 2(a). At elevated $T = 0.5$, $\Sigma''(\omega, k)$ remains k independent in roughly the same ω regime as in the $T = 0.1$ case. Nevertheless, it shows substantial deviation from zero at frequencies at and below the polaron band, indicating the importance of incoherent processes. The general trend in terms of the temperature dependence, seen in Figs. 3(c) and 3(d), qualitatively agrees with results based on the dynamical mean-field calculations [19].

C. Frequency moments

The aim of this section is to check the accuracy of our approach by computing the first three frequency moments of the spectral function. As already shown in Refs. [16,27], frequency moments of the single-polaron spectral function can be obtained analytically using the following relation:

$$\begin{aligned} M_m(k) &= \int_{-\infty}^{\infty} \omega^m A(\omega, k) d\omega \\ &= \langle [[[c_k, H], H], \dots, H] c_k^\dagger \rangle_T, \end{aligned} \quad (7)$$

where $\langle \dots \rangle_T$ represents the thermal average over zero-electron states and the number of commutators corresponds to the order of the frequency moment. Analytical expressions may be thus obtained for arbitrary moments even at finite T .

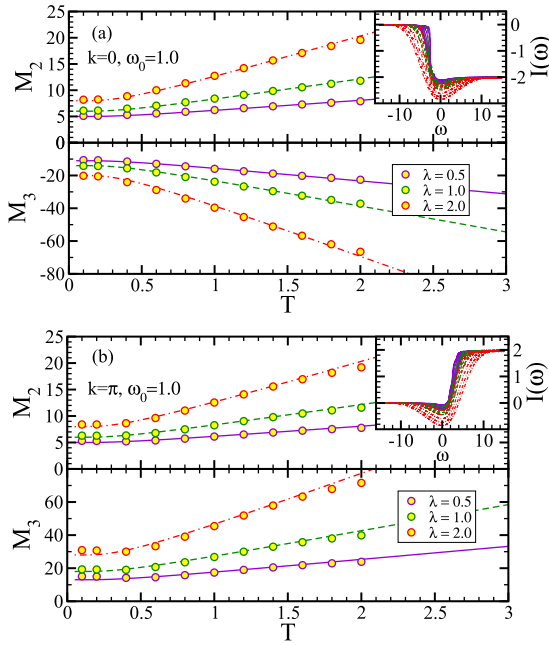


FIG. 4. M_2 and M_3 for different values of λ vs T for $k = 0$ in (a) and π in (b). Open symbols represent moments obtained from numerical results of $A(\omega, k)$, where instead of Lorentzian broadening we have used a Gaussian one with $\sigma = 0.05$ to ensure convergence of integrals. The lines represent analytical results given by Eqs. (8). Insets: $I(\omega)$ for different values of λ and $k = 0$ in (a) and π in (b). There are six curves for each set of λ and k computed at values of $T \in [0.2, 0.6, \dots, 1.8, 2.0]$. Plots were obtained by straightforward numerical integrations of $A(\omega, k)$, such as presented in Figs. 1 and 5.

Here we list just a few:

$$\begin{aligned} M_1(k) &= \epsilon(k), & M_2(k) &= \epsilon^2(k) + g^2(2n + 1), \\ M_3(k) &= \epsilon^3(k) + 2g^2\epsilon(k)(2n + 1) + g^2\omega_0, \end{aligned} \quad (8)$$

where $\epsilon(k) = -2t_0 \cos(k)$ and $n = 1/[\exp(\omega_0/T) - 1]$ is the Bose-Einstein distribution function. Note that $M_1(k)$ depends only on the wave vector k . In the insets of Fig. 4 we plot $I(\omega) = \int_{-\infty}^{\infty} \omega' A(\omega', k) d\omega'$ for different λ and T as well as two values of $k = 0$ and π . Note that all curves, in accordance with the first frequency moment $M_1(k)$, irrespective of λ and T , merge into two distinct values ± 2 in the large- ω limit. There is yet another universal consequence of M_1 that limits the temperature evolution of the density of states $N(\omega) = \frac{1}{L} \sum_k A(\omega, k)$. The center of the distribution $\int_{-\infty}^{\infty} \omega N(\omega) d\omega = \sum_k \epsilon(k) = 0$ remains independent of essentially all parameters of the system, as well as of T .

We now turn to the second and third moments of $A(\omega, k)$. In Figs. 4(a) and 4(b) we plot M_2 and M_3 at $k = 0$ and π , respectively. We find good agreement with analytical results given in Eqs. (8) up to $T \sim 2.0$, where moments, extracted from $A(\omega, k)$, start deviating from exact results due to a limited number of phonon excitations in our Hilbert space. It should be noted that when using M -Lanczos steps, the Lanczos procedure leads to results of $A(\omega, k)$ that have correct frequency moments up to the M th moment [25,26], and we have used $M = 500$ in our calculations. This may lead to a conclusion that comparing moments with analytical results

represents a trivial test. However, since the calculation is performed on a finite system with a limited size L as well as a limited number of phonon quanta, computed moments are also influenced by the limited Hilbert space. In contrast, analytical results in Eqs. (8) are exact in the thermodynamic limit.

IV. SUMMARY

To conclude, using the finite- T Lanczos method, adapted to the calculation of the Holstein polaron problem, we computed the polaron spectral function at finite T in all three EP coupling regimes, from the weak- to the strong-coupling one. Even though we had to limit the system size to a relatively small ring of $L = 6$ sites in order to allow a sufficient number of phonon excitations to obtain accurate results at elevated T , our results at small T compare well with those in the existing literature (see, for example, Refs. [10,14,16]). With increasing T additional features in the spectral function emerge already at temperatures below the phonon frequency due to processes where an electron annihilates one or more thermally excited phonons. Such effects should be taken into account when analyzing experimental data. More specifically, we observe a substantial shift of spectral weight towards lower as well as higher frequencies while the center of the spectra remains unchanged as it is set by the first frequency moment. Irrespective of EP coupling, the QP peak broadens with increasing T . In the weak-coupling regime the QP peak merges with the continuum around $T \sim \omega_0$ and becomes indistinguishable from the background. In contrast, in the strong-coupling regime the whole low- T structure of the spectral function remains well resolved even at high T . In addition, new peaks that emerge with increasing T below the frequency of the QP peak, spaced by $n\omega_0$, also remain distinguishable up to the highest T used in our calculations. The effective polaron mass m^* is weakly T dependent at small $\omega_0 = 0.5$ and shows nonmonotonic T dependence. At larger $\omega_0 \geq 1$, m^* increases with T . The self-energy remains k independent even at elevated T in the frequency range corresponding to the polaron band, while at higher frequencies it develops a distinguishable k dependence.

ACKNOWLEDGMENTS

J.B. acknowledges the support from program P1-0044 of the Slovenian Research Agency. J.B. and S.A.T. acknowledge support from the Center for Integrated Nanotechnologies, a U.S. Department of Energy, Office of Basic Energy Sciences, user facility. S.A.T. acknowledges support from LDRD. M.B. acknowledges funding from the Natural Sciences and Engineering Research Council of Canada. M.B. and J.B. also acknowledge funding from the Stewart Blusson Quantum Matter Institute. J.B. also acknowledges the hospitality of Dr. M. Stout.

APPENDIX A: SPECTRAL FUNCTION AT $k = \pi$

In Fig. 5 we show $A(\omega, k = \pi)$ for the same parameters as in Fig. 1. In all cases QP peaks possess very small QP weights, in accordance with previous zero- T results [2,10]. In the weak

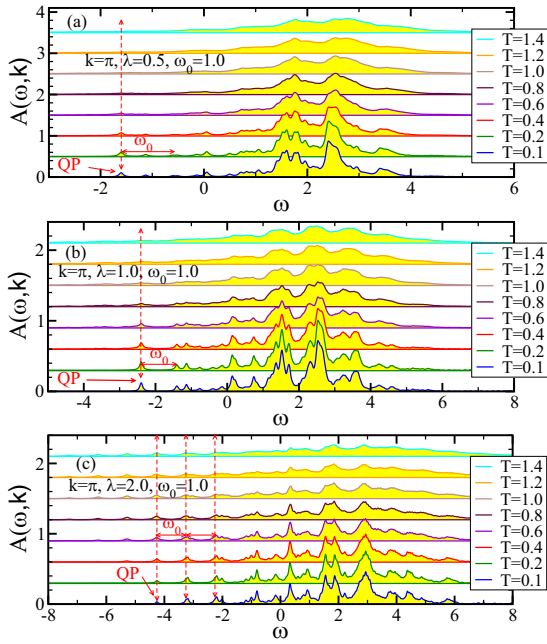


FIG. 5. $A(\omega, k = \pi)$ at $\omega_0 = 1.0$ computed for $\lambda = 0.5$ through $\lambda = 2.0$ from (a) to (c). The rest is the same as in Fig. 1.

and intermediate EP coupling regime, as shown in Figs. 5(a) and 5(b), their spectral weights decrease with increasing T until around $T \sim \omega_0$, where the QP peaks become nearly indistinguishable from the background. In the strong-coupling regime well-defined peaks spaced by ω_0 emerge below the QP peak with increasing T , as seen in Fig. 5(c). In contrast to the $k = 0$ case we observe only a slight increase of the spectral weight below QP peaks with increasing T . In order to gain further insight into the structure of $A(\omega, k = \pi)$, where at small $\lambda = 0.5$ most of the spectra are located in the vicinity of $\omega = 2$, we note that in the case of the free electron, there is a single peak at $\omega = 2$. At small λ and small or finite temperature, $A(\omega, k = \pi)$ becomes a (split) peak at $\omega = 2$. However, in the thermodynamic limit and small λ , the main peak at $\omega = 2$ has a nonzero width even at $T = 0$, from phonon emission. In contrast, for $A(\omega, k = 0)$, the main peak at $\omega = -2$ develops a nonzero width only as temperature increases, and phonons populate the initial state.

APPENDIX B: FINITE-SIZE ANALYSIS

In Fig. 6 we present results obtained for two different systems with $L = 6$ and 12 sites. On a smaller system we were able to use a larger maximal number of phonon quanta $N_{\max} = 22$; on the latter we were able to use only $N_{\max} = 16$. On a smaller $L = 6$ system we were able to reach much larger $T \sim \omega_0$ since the generated Hilbert space allowed for the maximal number of phonons per site, $n_{\max} \sim 3.7$, while the larger system had only $n_{\max} \sim 1.3$. In both cases $A(\omega, k)$ were computed on discrete k points according to periodic as well as twisted boundary conditions, equivalent to $k_{n,m} = 2\pi n/L + m\theta$, with $n \in [-L/2, L/2]$ and $\theta = 2\pi/(M_\theta L)$; $m \in [0, M_\theta - 1]$. For $L = 6$ and 12 systems we have chosen $M = 8$ and 4 , respectively. As a result, for each system size

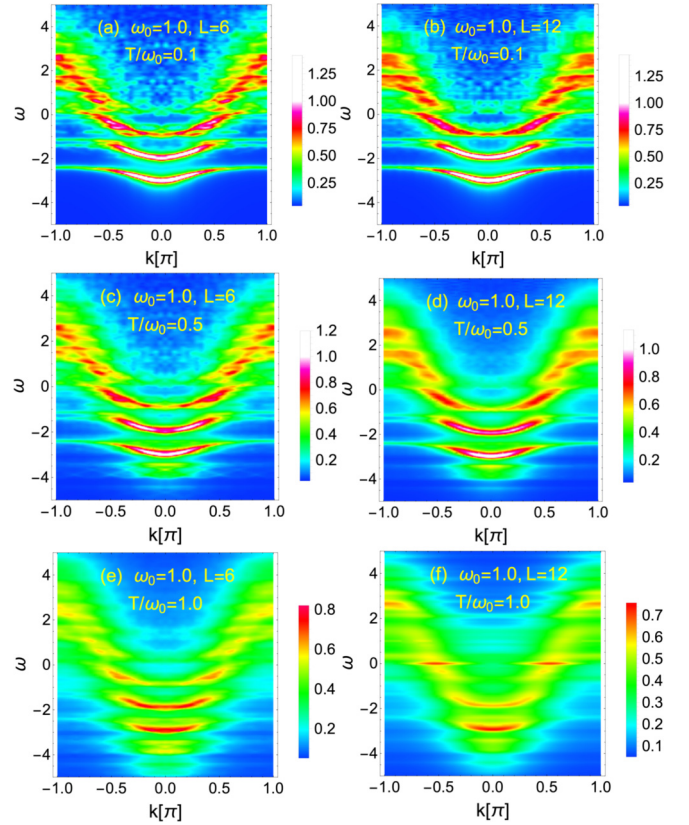


FIG. 6. $A(\omega, k)$ for $\lambda = \omega_0 = 1$ for two different system sizes, $L = 6$ in (a), (c), and (e) and $L = 12$ in (b), (d), and (f), and three different values of T/ω_0 as specified in plots. In all cases $A(\omega, k)$ was computed in 25 equally spaced nonequivalent k points in the interval $k \in [0, \pi]$ with increments of $\Delta k = \pi/24$. Note that in all plots from (a) to (f) the same color coding was used to enable direct comparison between different cases.

$A(\omega, k)$ were computed using $M_\theta * L/2 + 1$ nonequivalent k points. Despite substantially different system sizes results are qualitatively identical at low and high $T/\omega_0 = 0.1$ and 0.5 , respectively. As an independent check of our method we can also report excellent agreement with other methods, optimized for calculation at zero T . More specifically, we found good agreement of Figs. 6(a) and 6(b) with results of the same quantity computed at zero T presented in Fig. 4 of Hohenadler *et al.* [10] and Fig. 20(b) by Goodvin *et al.* [16].

Comparing results obtained on two different systems, we find good agreement in the low- T regime, i.e., for $T/\omega_0 \lesssim 0.5$ [see Figs. 6(a) and 6(b) as well as 6(c) and 6(d)]. More substantial differences appear at $T/\omega_0 = 1$, where due to the Bose-Einstein distribution increased $n_{\max} \gtrsim 1$ is needed to properly describe $A(\omega, k)$ at higher T . Note that in the $L = 12$ system n_{\max} is only $1/3$ of n_{\max} in the $L = 6$ system. This may be the reason that in Fig. 6(f) an unexpected (unphysical) increase of the spectral weight at $\omega \sim 0$ is observed in addition to a much smaller spectral weight below the polaron band in comparison to Fig. 6(e). This was the main reason to present our results on a smaller $L = 6$ sites system that allowed reliable results up to a higher $T/\omega_0 = 1$.

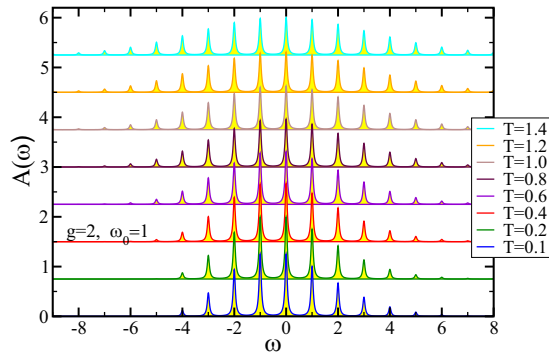


FIG. 7. $A(\omega)$ obtained from Eqs. (C4) and (C5) using $g = 2$ and $\omega_0 = 1$, where sums were taken up to $n, m = 30$. Note that the temperatures are given in units of ω_0 . Lorentzian broadening was used with $\eta = 0.05$.

APPENDIX C: SINGLE-SITE SPECTRAL FUNCTION

We first note that an expression for the single-site Holstein polaron spectral function at finite temperature was given in Ref. [19]. We present here a detailed derivation.

We start with the single-site problem described by the Hamiltonian

$$H_1 = g\hat{n}(a^\dagger + a) + \omega_0 a^\dagger a, \quad (\text{C1})$$

where \hat{n} represents the electron occupation number operator. In the case when $n = 1$ solutions are well-known coherent states $|\tilde{g}\rangle$, $\tilde{g} = g/\omega_0$, given by the condition

$$(a + \tilde{g})|\tilde{g}\rangle = 0,$$

$$|\tilde{0}\rangle = |\tilde{g}\rangle = e^{-\tilde{g}^2/2} \sum_{m=0}^{\infty} \frac{(-\tilde{g})^m}{\sqrt{m!}} |m\rangle, \quad (\text{C2})$$

with energy $\epsilon_0^{(1)} = -\omega_0 \tilde{g}^2$, while excited coherent states are given by

$$|\tilde{m}\rangle = \frac{(a^\dagger + \tilde{g})^m}{\sqrt{m!}} |\tilde{0}\rangle, \quad (\text{C3})$$

with corresponding energies $\epsilon_m^{(1)} = -\omega_0 \tilde{g}^2 + m\omega_0$. The spectral function $A(\omega)$ obtained from Eqs. (3) and (4) of the text manuscript simplified to a single-site problem is then given by

$$A(\omega) = \mathcal{Z}^{-1} \sum_{n,m=0}^{\infty} e^{-\beta\omega_0 n} |\langle \tilde{m}|n\rangle|^2 \delta[\omega + \omega_0(\tilde{g}^2 - m + n)], \quad (\text{C4})$$

where $\langle \tilde{m}|n\rangle$ represents the projection of the excited coherent state $|\tilde{m}\rangle$ onto a phonon state $|n\rangle$, given by

$$\langle \tilde{m}|n\rangle = e^{-\tilde{g}^2/2} \sum_{l=0}^{\min(m,n)} (-1)^{n-l} \tilde{g}^{n+m-l} \frac{\sqrt{m!n!}}{l!(m-l)!(n-l)!}. \quad (\text{C5})$$

Equations (C4) and (C5) in the limit $T \rightarrow 0$ simplify to a well-known result [34]:

$$A(\omega) = e^{-\tilde{g}^2} \sum_{m=0}^{\infty} \frac{\tilde{g}^{2m}}{m!} \delta[\omega + \omega_0(\tilde{g}^2 - m)]. \quad (\text{C6})$$

In Fig. 7 we present $A(\omega)$ for the single-site problem.

-
- [1] T. Holstein, *Ann. Phys. (NY)* **8**, 325 (1959).
[2] J. Bonča, S. A. Trugman, and I. Batistić, *Phys. Rev. B* **60**, 1633 (1999).
[3] L. C. Ku, S. A. Trugman, and J. Bonča, *Phys. Rev. B* **65**, 174306 (2002).
[4] S. Engelsberg and J. R. Schrieffer, *Phys. Rev.* **131**, 993 (1963).
[5] J. Ranninger and U. Thibblin, *Phys. Rev. B* **45**, 7730 (1992).
[6] F. Marsiglio, *Phys. Lett. A* **180**, 280 (1993).
[7] A. S. Alexandrov, V. V. Kabanov, and D. K. Ray, *Phys. Rev. B* **49**, 9915 (1994).
[8] H. Fehske, J. Loos, and G. Wellein, *Z. Phys. B* **104**, 619 (1997).
[9] H. Fehske, J. Loos, and G. Wellein, *Phys. Rev. B* **61**, 8016 (2000).
[10] M. Hohenadler, M. Aichhorn, and W. von der Linden, *Phys. Rev. B* **68**, 184304 (2003).
[11] G. De Filippis, V. Cataudella, V. Marigliano Ramaglia, and C. A. Perroni, *Phys. Rev. B* **72**, 014307 (2005).
[12] N. V. Prokof'ev and B. V. Svistunov, *Phys. Rev. Lett.* **81**, 2514 (1998).
[13] V. Cataudella, G. De Filippis, A. S. Mishchenko, and N. Nagaosa, *Phys. Rev. Lett.* **99**, 226402 (2007).
[14] B. Lau, M. Berciu, and G. A. Sawatzky, *Phys. Rev. B* **76**, 174305 (2007).
[15] M. Berciu and G. L. Goodvin, *Phys. Rev. B* **76**, 165109 (2007).
[16] G. L. Goodvin, M. Berciu, and G. A. Sawatzky, *Phys. Rev. B* **74**, 245104 (2006).
[17] E. V. L. de Mello and J. Ranninger, *Phys. Rev. B* **55**, 14872 (1997).
[18] S. Paganelli and S. Ciuchi, *J. Phys.: Condens. Matter* **18**, 7669 (2006).
[19] S. Ciuchi, F. de Pasquale, S. Fratini, and D. Feinberg, *Phys. Rev. B* **56**, 4494 (1997).
[20] A. S. Mishchenko, N. Nagaosa, G. De Filippis, A. de Candia, and V. Cataudella, *Phys. Rev. Lett.* **114**, 146401 (2015).
[21] T. Fulton, *Phys. Rev.* **103**, 1712 (1956).
[22] Y. Ōsaka, *Prog. Theor. Phys.* **22**, 437 (1959).
[23] M. Saitoh, *J. Phys. Soc. Jpn.* **49**, 878 (1980).
[24] M. Kang, S. W. Jung, W. J. Shin, Y. Sohn, S. H. Ryu, T. K. Kim, M. Hoesch, and K. S. Kim, *Nat. Mater.* **17**, 676 (2018).
[25] J. Jaklič and P. Prelovšek, *Adv. Phys.* **49**, 1 (2000).
[26] P. Prelovšek and J. Bonča, *Ground State and Finite Temperature Lanczos Methods*, Springer Series in Solid-State Sciences Vol. 176 (Springer, Berlin, 2013), Chap. 1, pp. 1–30.
[27] P. E. Kornilovitch, *Europhys. Lett.* **59**, 735 (2002).
[28] B. S. Shastry and B. Sutherland, *Phys. Rev. Lett.* **65**, 243 (1990).
[29] D. Poilblanc, *Phys. Rev. B* **44**, 9562 (1991).

- [30] J. Bonča and P. Prelovšek, *Phys. Rev. B* **67**, 085103 (2003).
- [31] L.-C. Ku and S. A. Trugman, *Phys. Rev. B* **75**, 014307 (2007).
- [32] O. S. Barišić, *Phys. Rev. B* **73**, 214304 (2006).
- [33] More work is needed to confirm these m^* results, especially at low phonon frequency, due to the decreasing QP lifetime (widening of the QP peak).
- [34] G. D. Mahan, *Many-Particle Physics* (Plenum, New York, 1990).